Food Chemistry: X 25 (2025) 102170

Contents lists available at ScienceDirect

Food Chemistry: X

journal homepage: www.sciencedirect.com/journal/food-chemistry-x

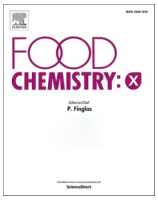

Wet pulverization combined with temperature cycling strategy for extraction of *Stropharia rugosoannulata* protein with attenuating hepatic steatosis on obese mice

Peng Liu [a,1], Chen Gao [a,b,1], Wen Li [a], Wanchao Chen [a], Zhong Zhang [a], Di Wu [a], Tingzhao Li [c,d], Shuai Sun [c,*], Yan Yang [a,*]

[a] *Institute of Edible Fungi, Shanghai Academy of Agricultural Sciences, Key Laboratory of Edible Fungi Resources and Utilization (South), Ministry of Agriculture, P. R. China, National Engineering Research Center of Edible Fungi, Shanghai 201403, China*
[b] *University of Shanghai for Science and Technology, Shanghai 200093, China*
[c] *Amway Innovation & Science Co, Ltd, Shanghai 201203, China*
[d] *Amway Botanical R&D Center, Wuxi 214115, China*

ARTICLE INFO

Keywords:
Stropharia rugosoannulata
Obesity
Protein
Hepatic steatosis
Preparation strategy

ABSTRACT

Stropharia rugosoannulata is an edible fungus with high protein content and excellent bioactivities. However, the effective extraction of *S. rugosoannulata* protein has been a challenge, and the amelioration of it against obesity still remain unclear. Herein, *S. rugosoannulata* protein (SRA) with mainly molecular weight of 15, 40 and 50 kDa, complete amino acid composition and typical α-helix structure, was obtained by wet pulverization combined with temperature cycling strategy. SRA alleviated the pathological progression in obese mice induced by high-fat diet via regulating lipid metabolism in liver and adipose tissues. SRA could obviously improve hepatic steatosis, which may be attributed to inhibiting MAPK/PGC-1α pathway. Moreover, SRA repaired the cross-talk between gut microbiota and liver via modulating intestinal microecology, and restoring the integrity and function of the intestinal barrier in obese mice. This study highlights an efficient and easy strategy for preparing *S. rugosoannulata* protein and its effects against obesity.

1. Introduction

Obesity is one of the most common metabolic disease with increasing prevalence, which causes a global health concern, due to the significant correlation between obesity and many chronic diseases such as hyperlipidemia, hyperglycemia, and hypertension related to coronary artery disease (Li, Wu, Liu, & Yang, 2020). Obesity is characterized in the excessive or inappropriate fat accumulation, partially accompanied by elevated liver triglycerides (i.e., hepatic steatosis) (Bray, Kim, Wilding, & World Obesity, 2017; Liu et al., 2023). Therefore, obesity is a risk factor for developing nonalcoholic fatty liver disease, which can further pose hepatitis, hepatic fibrosis, dyslipidemia, and may induce liver cancer. There is evidence that the morbidity of hepatic steatosis reaches up to 80 % in obese individuals (Spagnuolo et al., 2019). Alleviating obesity is an effective strategy to reduce nonalcoholic fatty liver disease, fatty liver and other metabolic diseases. Recent studies described a close interaction between dietary, gut and liver metabolism, with pathways involving intestinal permeability, the composition of gut microbiota and systemic inflammation, etc. (Di Ciaula et al., 2020). Therefore, modulation of the gut-liver crosstalk in obesity opens an avenue for targeted intervention in the future. Currently, some strategies to improve obesity, such as increasing energy expenditure and reducing dietary intake, are difficult to persist in the long term. There is accumulating evidence regarding the importance of diet for health across the lifespan, functional foods as the basic building blocks of our biology play both the roles of food and beneficial health. The utilization of potent natural nutrients as a novel approach for the prevention and treatment of obesity is in line with current strategies.

Edible fungi are considered as food with nutritional functions and a source of physiologically beneficial molecules. *Stropharia rugosoannulata* is a popular edible and medicinal fungus with a long history of usage. Numerous studies have explored that *S. rugosoannulata* possessed

* Corresponding author.
E-mail addresses: sunshuai_amway@163.com (S. Sun), yangyan@saas.sh.cn (Y. Yang).
[1] Peng Liu and Chen Gao contributed equally to this work.

https://doi.org/10.1016/j.fochx.2025.102170
Received 7 August 2024; Received in revised form 28 December 2024; Accepted 7 January 2025
Available online 11 January 2025

widespread nutrients, such as proteins, carbohydrates, lipids, vitamins, inorganic salts, and dietary fiber, etc., and simultaneously exerted various bioactivities (Gao et al., 2022; W. Li et al., 2022). It was reported that edible fungi protein usually displayed a complete essential amino acid profile, met dietary requirements, and provided health advantages by eliciting antioxidant over animal proteins (Ayimbila & Keawsompong, 2023). Moreover, the peptides prepared from *S. rugosoannulata* could exert excellent antihypertensive effect via binding to the amino acid residues in the angiotensin-converting enzyme active pocket (W. Li et al., 2022). However, the relevant research of protein component from *S. rugosoannulata* is still unclear, especially its effect on obesity.

Currently, the solvent-assisted methods using organic, alkali and acid are common strategies for protein extraction, while most of them face the challenge of contaminating easily and complex solvent removal process. Other methods such as ultrasonic and microwave are difficult to adapt to industrial preparation, because of the complex equipment and high costs. Wet pulverizing strategy is widely used to prepare nanofibers of cellulose or depolymerize the polysaccharide, which could overcome the disadvantages, such as low efficiency and solvent pollution. Additionally, temperature cycling method has been regarded as a residue-free and cost-effective tool for improving protein functional properties (Xu et al., 2023). Tiwari SC et al. isolated microtubule associated proteins from cells and tissues by applying temperature cycling method based on the characteristics of protein solubility changing with temperature (Tiwari & Suprenant, 1993). However, research on the application of wet pulverization systems combined with temperature cycling method in mushroom protein extraction is rare.

Accordingly, in this study, wet pulverization strategy combined with temperature cycling method was employed to obtain protein-riched extraction from *S. rugosoannulata* (SRA). Moreover, the reversal effect and molecular mechanism of SRA on high-fat diet induced obesity in vitro and in vivo were explored. Based on the gut-liver axis theory, the effects of SRA in gut microbiota and intestinal barrier function were analyzed simultaneously. This study will indicate the controlling effect and action mechanism of SRA derived from *S. rugosoannulata* on obesity, which provides a theoretical basis for the development and utilization of functional proteins of *S. rugosoannulata*.

2. Materials and methods

2.1. Materials

S. rugosoannulata was stored in Institute of Edible Fungi, Shanghai Academy of Agricultural Sciences. Oil red O staining solution was obtained from Shanghai yuanye Bio-Technology Co., Ltd. (Shanghai China). SYBR was bought from Thermo Scientific (Waltham, MA, USA). Oleic acid was purchased from Beyotime Biotechnology (Shanghai China). The antibodies of F4/80, PGC-1α, HNF-4α, PPAR-α, SREBP, ERK1/2, P-ERK1/2, JNK, P-JNK, P38, P—P38 and β-actin were purchased from Cell Signaling Technology (Danvers, MA, USA).

2.2. Preparation and process optimization of the S. Rugosoannulata protein (SRA)

Concretely, 200 g fruiting bodies of fresh *S. rugosoannulata* fruiting bodies was placed at −20 °C, 5 °C, and 25 °C for 6 h respectively, and then placed at 25 °C for 4 h, repeat two times. It was crushed with distilled water (1.0 L) using high pressure homogenization. The liquid was centrifuged at 8000 rpm (10 min) to obtain the supernatant. Ultrafiltration on the supernatant was performed to obtain components with a molecular weight greater than 10,000 Da. Then the protein was subsequently precipitated from the supernatant by salting out with a series of ammonium sulfate concentrations, including 40 %, 50 %, 60 %, and 70 %. After that, it was centrifuged at 10,000 rpm (30 min) to obtain the precipitation. The samples were placed in dialysis buffer to intercept molecular weights greater than 3500 Da, and dialysis at 4 °C for at least 72 h, followed by lyophilized to yield the *S. rugosoannulata* protein (SRA).

2.3. Characterization of SRA

2.3.1. Protein content, SEM and particle size analysis

The protein content of SRA was analyzed by the Dumas combustion method (Marco, Rubio, Compano, & Casals, 2002). The ultrastructural features of SRA were collected using a scanning electron microscopy (SEM) (Zeiss, Oberkochen, Germany). The particle size of SRA was determined by a NanoBrook 90Plus PALS nanoparticle size zeta potential meter.

2.3.2. Amino acids and molecular weight analysis

The amino acids analysis of SRA was conducted. In brief, added 6 mol/L hydrochloric acid solution 10 mL in the hydrolysis tube, dropped in phenol 3–4 drops and mixed in vortex. Then filled it with nitrogen for 3 times and tighten the screw cap immediately. The covered hydrolysis tube was placed at 110 °C for 22 h. Filtered the hydrolysate through a filter paper into a 50 mL volumetric flask, precisely absorbed 1 mL of the above filtrate, evaporated until nearly dry (repeat three times). Finally added 1 mL Sodium Citrate buffer solution ($pH = 2.2$), passed through 0.22 μm filter membrane for amino acid determination using HPLC (Agilent 1100, USA). The molecular weight determination of SRA was used sodium dodecylsulfate-polyacrylamide gel electrophoresis (SDS-PAGE).

2.3.3. FT-IR and CD analysis

The Fourier transform infrared (FT-IR) spectra of SRA sample was obtained using a Nicilet Is20 infrared spectrometer with a wave number range of 4000–400 cm^{-1}. The sample was added into 0.1 cm path length quartz cuvettes for the detection of circular dichroism (CD) spectra at 190–250 nm using Biologic New MOS-450CD spectrometer.

2.4. Cell culture and treatment

L-O2 cells were cultured in RPMI 1640 medium supplemented with 10 % fetal bovine serum at 37 °C in a humidified 5 % CO_2 environment. Cells were added into 96-well culture plate, after 24 h, cells were incubated with serum-free medium containing 1.0 mM OA. Simultaneously, SRA with different concentration (SRAL: 50 μg/mL, SRAM: 100 μg/mL, SRAH: 200 μg/mL) was added to the medium for 24 h. The lipid content in cells was detected by oil red O staining, and visualized through an inverted optical microscope.

2.5. Animals

Male ICR mice (20 ± 2 g) were obtained from Shanghai SLAC Laboratory Animal Co., Ltd. Mice were fed in accordance with the Guide for the Care and Use of Laboratory Animals published by the National Institutes of Health and were approved by the related ethical regulations of Shanghai Academy of Agricultural Sciences (the ethical permission number: SAASPZ0423090).

2.5.1. Animal feeding

Mice were divided into five groups ($n = 5$ per group): CTL, HFD, SIM, SRAL and SRAH groups. Mice in the CTL group were received normal feed, all mice in the other groups were fed with high fat diet (60 % fat). Simultaneously, mice in the SRA groups were gavaged with SRA (SRAL: 400 mg/kg and SRAH: 1000 mg/kg), mice in the SIM group were filled with 8 mg/kg simvastatin, and mice in the CTL and HFD groups were received the same volume of distilled water, once a day for 6 weeks. The doses in SRAL and SRAH groups were separately equivalent to 44 and 110 mg/kg daily of human calculated based on body surface area.

2.5.2. Sample collection

Three days before concluding the experiment, feces were collected at regular intervals, and stored at −80 °C. After completing the experiment, all mice were anesthetized prior to cervical dislocation. Blood was then collected from the eye, centrifuged and stored. The liver, adipose and small intestine tissues were collected for subsequent hematoxylin-eosin (H&E) staining and other projects, respectively.

2.6. Biochemical analysis of serum and liver tissue

Serum total antioxidant capacity (T-AOC) and malondialdehyde (MDA), and the total cholesterol (TC) and triglycerides (TG) in liver tissue were detected according to kit instructions (Nanjing Jiancheng Bioengineering Institute, Nanjing, China).

2.7. Histopathological and immunohistochemistry analysis

After being buried in paraffin, it was sliced to produce paraffin tissue flakes. Then, they were analyzed by Hematoxylin & eosin staining (H&E) and immunohistochemical analysis. Positive areas were measured quantitatively by ImageJ software (NIH, USA).

2.8. Western blotting analysis

Whole protein was extracted from liver, thereby were separated and transferred to PVDF membranes. After antibody incubation, the target blots were visualized by ECL reagents (Beyotime Biotechnology, China)

2.9. qRT-PCR analysis

Total RNA was obtained with TRIzol for cDNA synthesis. The system included SYBR Green Master Mix, 10 nM primer pair (Table S1) and 0.2 μg cDNA. Relative mRNA levels were detected by real-time PCR system (QuantStudio™6 Flex, ABI), and analyzed by $2^{-(\triangle\triangle CT)}$ method.

2.10. 16S rRNA gene pyrosequencing and analysis

Total fecal bacterial genomic DNA from CTL, HFD, SIM, SRAL and SRAH groups was extracted by the cetyltrimethylammonium bromide/sodium dodecyl sulfate method. The V3-V4 region of 16S rRNA was amplified using the forward primers 341F-805R. Sequencing libraries were generated, and then sequenced on an Illumina Miseq platform. The sequences were clustered into bins called operational taxonomic units (OTUs) based upon similarity (Chen et al., 2020). The detailed data analysis referred to previous report (Liu et al., 2023).

2.11. Statistical analysis

All data were expressed as mean ± standard error. One-way analysis of variance (ANOVA) was performed. Normality and homogeneity of the results were evaluated by Shapiro-Wilk test. Significance is indicated as $p < 0.05$.

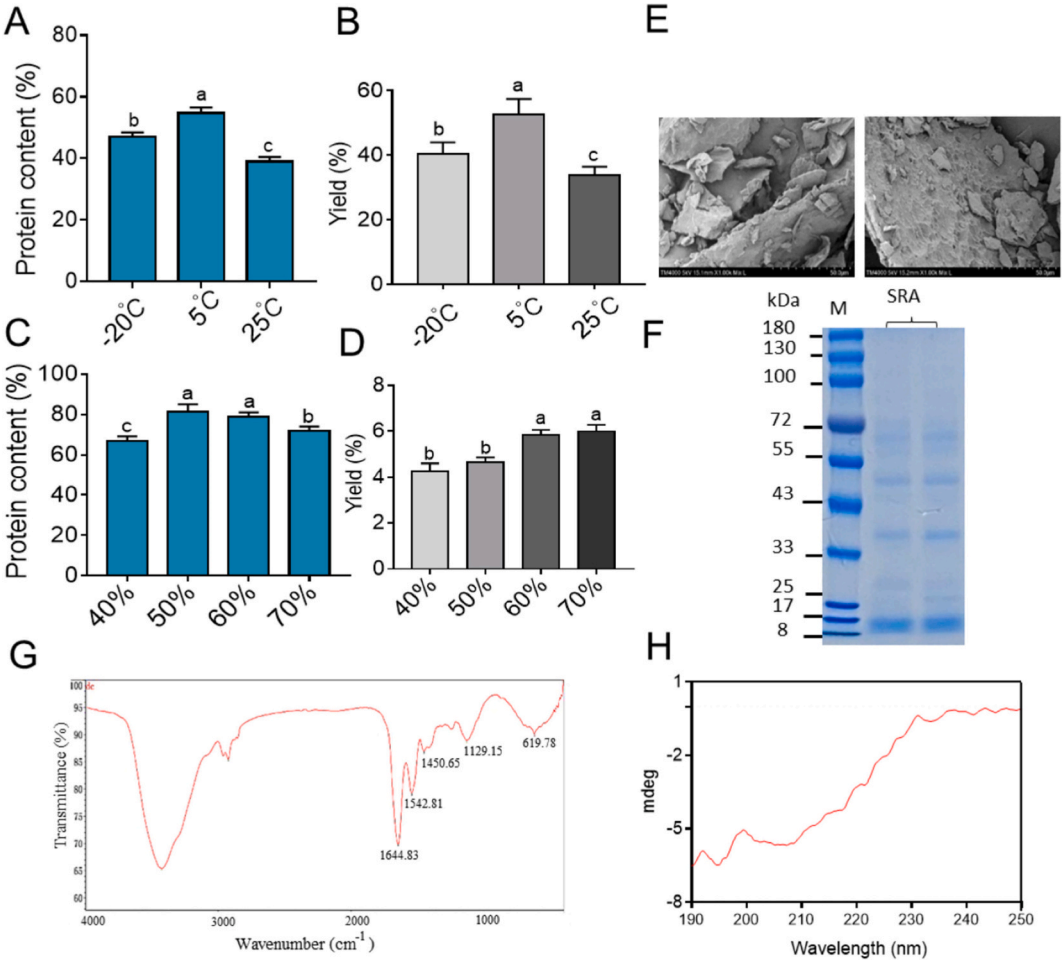

Fig. 1. Preparation and characterization of SRA. The protein content in SRA (A) and their yields (B) at different temperatures. The protein content in SRA (C) and their yields (D) at different concentration of ammonium sulphate. The SEM images (E), SDS-PAGE profile (F), FT-IR spectra (G) and CD spectra (H) were showed. All values are presented as means ± SEM ($n = 3$). In the same substance content, different letters represent statistical significance ($P < 0.05$).

3. Results and discussion

3.1. Preparation of SRA

SRA was extracted from *S. rugosoannulata* fruiting bodies via wet pulverization strategy combined with temperature cycling method in different temperatures. The results showed that SRA was processed at 5 °C with the highest protein content (54.40 %), compared to other treatment temperatures (Fig. 1A). Moreover, the data of yield also indicated that the yield of samples processed under 5 °C was 52.50 %, which was significantly higher than that of samples processed under −20 °C (40.48 %) and 25 °C (33.85 %) (Fig. 1B). The lower protein content obtained at −20 °C might be due to protein denaturation caused by freezing and thawing at low temperature and further lost by ultrafiltration. Previous studies proved that freeze can induce complex physical and chemical changes in the solvent/solute conditions, resulting in denaturation and degradation of proteins (Kolhe, Amend, & Singh, 2010). Herein, after temperature cycling from 5 °C to 25 °C, the protein content was increased, which might be attributed to the enhanced cell sensitivity at 5 °C due to factors such as shrinkage and re-expansion of cells, and changes in intracellular electrolyte concentration, playing a pivotal role in cell wall damage and protein release. Because of protein solubility affected by ions, the ammonium sulfate was used to isolated protein fraction and its addition concentration was optimized in this study. The results showed that ammonium sulfate-induced salting-out could isolate and purify SRA, evidencing that the protein content was significant increased, especially at concentrations of 50 % and 60 %, where the protein content reached approximately 80 % (Fig. 1C). Comparative studies of the yield demonstrated that the yields under 60 % and 70 % concentration ammonium sulfate treatment were significantly higher than that under 40 % and 50 % concentration (Fig. 1D). In conclusion, 60 % ammonium sulfate was employed to isolate SRA with the higher protein content (79.08 %) and yield (5.89 %).

3.2. Characterization of SRA

3.2.1. Morphological characteristics, molecular weight and amino acid composition analysis

SEM was widely applied in the surface morphology of biomacromolecules. The microstructure of SRA exhibited irregular block, a surface with several fragments, stratified structure and slight potholes (Fig. 1E). The average particle distribution of SRA in deionized water exhibited a narrow and symmetrical signal around (266.91 ± 2.70) nm. SRA was separated by SDS-PAGE, and the results showed four main bands at 70, 50, 40 and 15 kDa apparent molecular mass, approximately. The 15 kDa protein seemed to account for a larger proportion of the SRA, compared to other protein bands (Fig. 1F). Amino acid compositions of SRA were analyzed and the data showed in Table 1. 17 amino acids were identified, in which glutamate, aspartate, leucine and alanine were dominant amino acids in SRA, accounting for 15.89 %, 13.01 %, 9.85 % and 8.13 %. It was reported that glutamate as one of the most abundant of the amino acids played critical roles in nutrition, metabolism and signaling. For example, it is of fundamental importance to synthesis the glutathione and the polyglutamated folate cofactors (Brosnan & Brosnan, 2013). Additionally, SRA contained a quantity of essential amino acids as well, including lysine, phenylalanine, isoleucine, leucine, valine and methionine. The most abundant essential amino acid was leucine, followed by valine. Edible mushroom proteins generally possess complete essential amino acid, are promising alternative proteins, compared to plant proteins lacking some essential amino acids (Gonzalez et al., 2020).

Table 1
Amino acid composition of SRA.

Amino acids	Relative amount (%)	Amino acids	Relative amount (%)
Aspartate (Asp)	13.01	Proline (Pro)	6.39
Threonine (Thr)	5.34	Tryptophan (Trp)	1.92
Serine (Ser)	4.31	Lysine (Lys) [a]	5.37
Glutamate (Glu)	15.89	Phenylalanine (Phe) [a]	1.25
Glycine (Gly)	6.73	Isoleucine (Ile) [a]	5.31
Alanine (Ala)	8.13	Leucine (Leu) [a]	9.85
Cysteine (Cys)	0.85	Valine (Val) [a]	8.16
Arginine (Arg)	3.48	Methionine (Met) [a]	1.01
Histidine (His)	3.02		

[a] : Represented essential amino acids.

3.2.2 FTIR and CD analysis.

To confirm the molecular structure of SRA, FTIR analysis was employed. It showed the typical absorption characteristics of protein (Fig. 1G). Near 1100 cm^{-1} was the C—O bond absorption peak, which was attributed to the protein molecule containing a pyran ring (Luo, Huang, Chen, Zong, & Lou, 2023). The characteristic peaks of 1450, 1542 cm^{-1} corresponding to N—H stretching, which were attributed to the protein molecule containing amides (Luo et al., 2023; Tatulian, 2019). The absorption peak near 1640 cm^{-1} was the carbonyl (C=O) stretching vibration or N—H variable angle vibration (J. Zhang et al., 2022). It was reported that the amide I mode occurred between 1700 and 1600 cm^{-1} and was generated primarily by the C=O stretching vibration, plus CN and CCN out-of-plane bending vibrations and minimally by the NH in-plane bending mode (S & J, 1978). The amide I mode was by far the most useful absorbance band in structural characterization of proteins and peptides (Tatulian, 2019). It is worth noting that the strong absorption in the 1644 cm^{-1} was might be contributions from the α-helix structure (Tatulian, 2019). CD spectra was further applied to analyze secondary structure of SRA. It indicated that a positive spectral peak at 192 nm, and a large negative band approximately between 205 and 210 nm were showed (Fig. 1H), which were speculated to be contributed by the characteristic bands of random coil at 200 nm and α-helix at 208 nm (Cao et al., 2023). Therefore, the secondary structure of SRA determined by CD spectroscopy was consistent with the results of FTIR, suggesting that α-helix might be the dominant secondary structure of SRA.

3.3. Regulation of adipocyte lipolysis of SRA in obese mice induced by high-fat diet

A high-fat diet induced hyperlipidemia mouse model was established to further investigate the hypolipidemic activity of SRA. The epididymal fat index of mice in the HFD group was also increased, while it was significantly reduced after SRAL and SRAH interventions (Fig. 2A). These data indicated that SRA can improve obesity symptoms caused by HFD. Generally, obese mice show typical characteristics of hyperlipidemia, such as high levels of TC and TG (Cong et al., 2021). Consistently, compared with healthy mice, the levels of TC and TG in serum of mice with a HFD treatment were obviously elevated, which were significantly higher than that of SRAL and SRAH treatments (Fig. 2B, C). Edible fungi with low energy were favorable for weight loss, and could admittedly improved obesity (Chang et al., 2015).

HFD can induce steatosis of adipose tissue and was related to various serious health risks. Edible fungi as low in fat are considered the the ultimate diet for treating obesity. Compared to the CTL group, the size of adipocytes in the HFD model was significantly enlarged, which was the main causes of obesity and increased adipose tissue (Fig. 2D-G). SRAL and SRAH interventions improved the aforementioned pathological symptom of adipocyte enlargement (Fig. 2D-G). To further investigate the regulatory effect of SRA on lipid metabolism in epididymal fat, the mRNA expression levels of related genes were measured. The results indicated that an obvious decline in acetyl-CoA carboxylase-1 (ACC-1), farnesoid X receptor (FXR), peroxisome proliferator-activated receptor

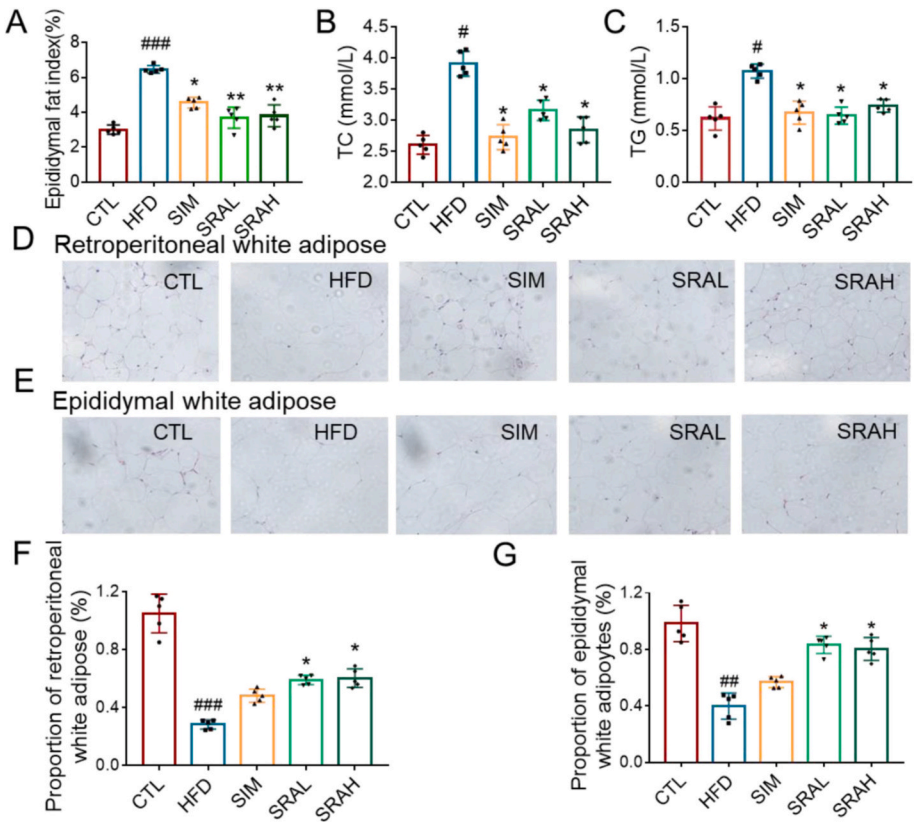

Fig. 2. SRA improved hyperlipidemia symptoms and adipocyte proliferation in obese mice induced by HFD. The epididymal fat index (A), and the levels of TC (B) and TG (C) were showed. H&E analysis of retroperitoneal white adipose tissue (200 ×) (D) and epididymal white adipose tissue (200 ×) (E), and positive staining areas were showed (F-G). All values are presented as means ± SEM ($n = 5$). Significantly different (*$P < 0.05$, **$P < 0.01$) versus the HFD group. Significantly different (#$P < 0.05$, ##$P < 0.01$, ###$P < 0.001$) versus the CTL group.

gamma coactivator-1 alpha (PGC-1α) and peroxisome proliferator-activated receptor gamma (PPAR-γ) expression was observed in the HFD group, whereas the expression levels of them were enhanced by SRAL and SRAH treatments (Fig. S1A—D). Moreover, the mRNA levels of uncoupling protein 1(UCP-1), sterol regulatory element-binding protein-1c (SREBP-1c), fatty acid binding protein 1 (FABP1) and hydroxy-3-methylglutaryl coenzyme A reductase (HMGCR) were upregulated in epididymal fat of mice fed a HFD, while they were reversed by SRAL and SRAH (Fig. S1E—H). Some edible fungi (such as *Kluyveromyces marxianus* and *Auricularia polytricha* etc.) possessed hypolipidemic effect by competitively inhibiting 3-hydroxy-3-methyl-glutaryl coenzyme A (HMG-CoA) reductase activity, which was responsible for the cholesterol biosynthesis (Xie et al., 2015; Zhao et al., 2015). Therefore, numerous studies have indicated that the mechanism of reducing cholesterol of these edible fungi was related to the regulation of cholesterol synthesis metabolism, such as regulation of lipoprotein lipase and diacylglycerol acyl-transferase activities (Sun et al., 2007). In summary, SRA played a critical role in regulating adipocyte differentiation and lipid deposition.

3.4. Moderation of SRA on hepatic steatosis in mice with obesity

3.4.1. Inhibition of lipid aggregation in vitro and in vivo

To investigate the hypolipidemic effects of SRA, an oleic acid induced hyperlipidemia model in L-O2 cells was adopted in vitro. Oil red O staining was performed on cells to explore the lipid accumulation. The results showed that the intracellular lipid droplet content in the OA group (oleic acid treatment) significantly increased, compared to the CTL group. SRA with a mass concentration in the range of 50–200 μg/mL can significantly reduce oleic acid induced lipid aggregation (Fig. 3A). The results preliminary indicated that SRA possessed an inhibitory effect on lipid aggregation in liver cells induced by oleic acid. Oil red O staining of the liver was further performed. SRAL and SRAH alleviated the hepatic lipid droplets compared with no-treatment HFD mice (Fig. 3B, D). This suggested that long-term consumption of a HFD induced the development of fatty liver in mice, while it can be relieved by SRA administration. Furthermore, HFD can cause certain liver injury in mice, as indicated by pathological damage, elevation of MDA level and decrease of T-AOC level. SRAL and SRAH treatments ameliorated pathological symptoms, such as inflammation, cell infiltration, and swelling in liver cells (Fig. 3C), and inhibited oxidative stress response in liver tissue by enhancing T-AOC level and reducing MDA level (Fig. 3E, F). Taken together, these results demonstrated that SRA administration evidently relieved hepatic fat accumulation and liver injury induced by HFD.

3.4.2. Regulation of lipid metabolism

To analysis the molecular mechanisms of SRA regulated hepatocytic lipid droplet aggregation on HFD induced mice, the levels of gene and protein related to lipid metabolism in liver were measured, including hepatocyte nuclear factor receptor-4α (HNF-4α), PPAR-α, SREBP-1, PPAR-γ, ACC-1, FXR, fatty acid synthetase (FASN) and cluster of differentiation 36 (CD36). Among them, HNF-4α plays a key role in improving diabetes and obesity via hydrolyzing triglycerides and inhibiting fat production (Y. Li et al., 2016). SREBP-1, PPARs ACC-1 and FXR are key factors that regulate numerous genes involved in lipid biosynthesis (Gu et al., 2022). Upregulation of PPAR-α level and the downregulation of SREBP-1 level could alleviate hepatic steatosis through permitting fatty acid transport into and oxidation in the mitochondrion (Jin et al., 2021). In this study, the protein levels of HNF-4α

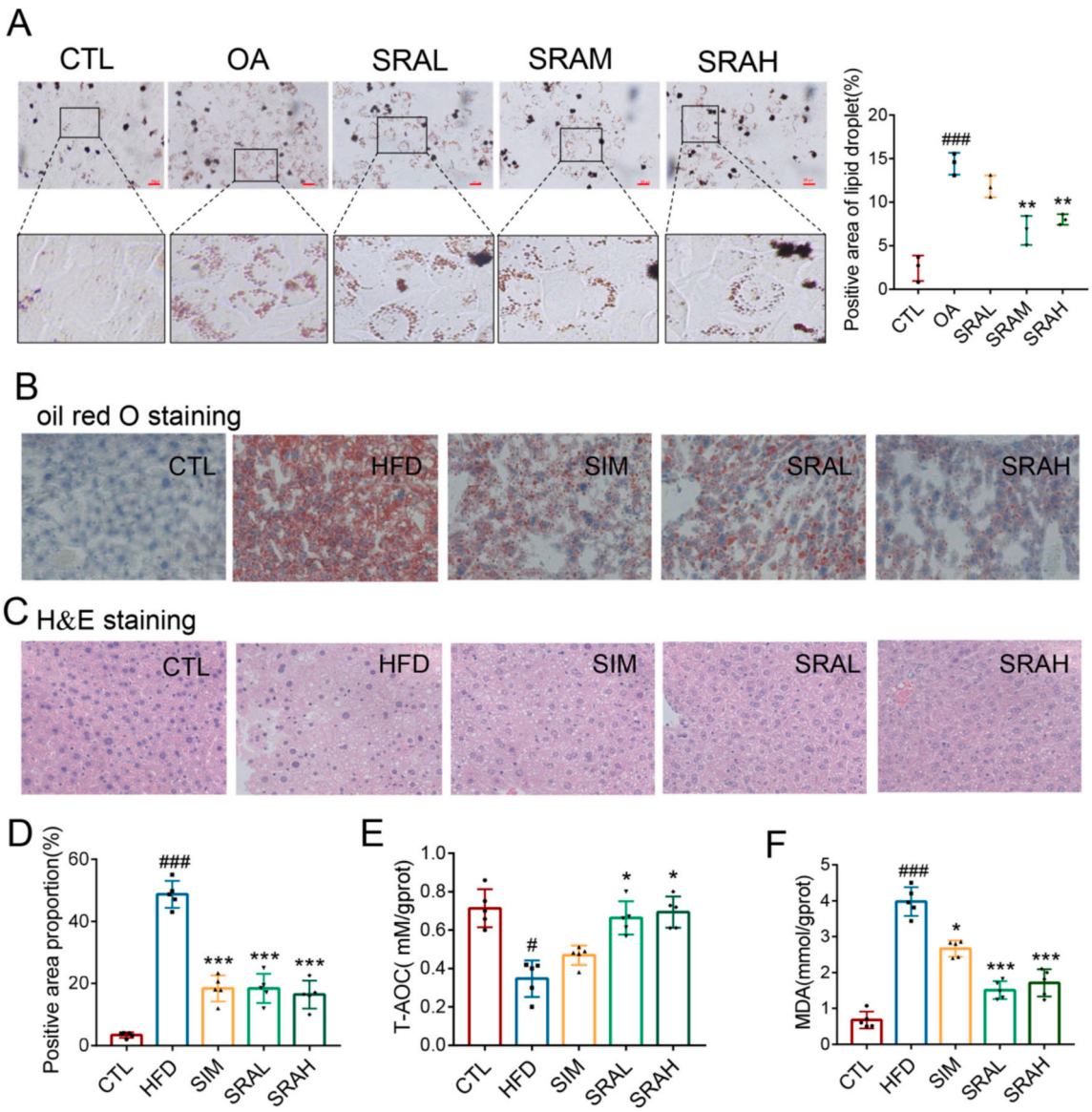

Fig. 3. SRA improved hepatic steatosis and liver function in obese mice. SRA inhibited lipid aggregation in L-O2 induced by oleic acid, Scale: 20 μm (A). Oil red (B) and H&E (C) staining of liver tissue were showed (200 ×), the positive staining areas of oil red staining was analyzed (D). The levels of T-AOC (E) and MDA (F) in liver tissue were detected. All values are presented as means ± SEM ($n = 5$). Significantly different ($^{*}P < 0.05$, $^{**}P < 0.01$, $^{***}P < 0.001$) versus the HFD or OA group. Significantly different ($\#P < 0.05$, $\#\#\#P < 0.001$) versus the CTL group. (For interpretation of the references to colour in this figure legend, the reader is referred to the web version of this article.)

and PPAR-α were significantly lower, and the protein level of SREBP-1 was evidently higher in HFD-fed mice than in the normal diet mice, while the levels of them were reversed by SRAL and SRAH treatments (Fig. 4A-F). Meanwhile, the results showed that the mRNA level of PPAR-α was down-regulated in HFD-induced mice, while it returned to basal levels in the SRAL and SRAH groups. SRA can increase the mRNA level of SREBP-1c in the liver tissue of mice induced by HFD (Fig. 4G, H). This result supported the aforementioned conclusion. Additionally, the mRNA levels of PPAR-γ, ACC-1, FXR, FASN and CD36 were also detected. The mRNA levels of ACC-1 and CD36 were elevated and the mRNA levels of PPAR-γ, FXR and FASN were diminished in HFD group compared with normal diet group, SRAL and SRAH treatments can reverse the mRNA levels of these genes (Fig. 4I-M). Herein, it was worth noting that SRA increased the mRNA levels of FASN and PPAR-γ in HFD-induced mice. Diniz TA et al. (Diniz et al., 2021) indicated that PPAR-γ upregulation could improve the machinery of lipid droplets expansion, while some studies have shown that ablation of PPAR-γ in hepatocytes had a protective effect against steatosis development under high-fat regimen. Additionally, lipogenic enzyme FASN participated in fatty acid uptake and de novo synthesis (M. Zhang et al., 2023). However, there are also different conclusion, it was reported that HFD treatment could decrease expression of encoding lipid metabolism genes FASN (Yan et al., 2022). Therefore, the regulation of lipid metabolism by PPAR-γ and FASN is complex, while the regulatory mechanism of SRA on them needs further exploration. In summary, the protection of SRA on HFD-induced obesity was attributed to regulating the expression of these genes related with lipid metabolism.

Accumulating evidences suggested that PGC-1α as a target for anti-obesity played a central role in the regulation of lipid metabolism (Cheng, Ku, & Lin, 2018; Liang & Ward, 2006). It was reported that cells with reduced PGC-1α can control expression of key enzymes in lipolysis and the glycerolipid/free fatty acid cycle, such as FXR and PPARs (Haemmerle et al., 2011; Oropeza et al., 2015; Y. Zhang, Castellani, Sinal, Gonzalez, & Edwards, 2004). To further explore the molecular

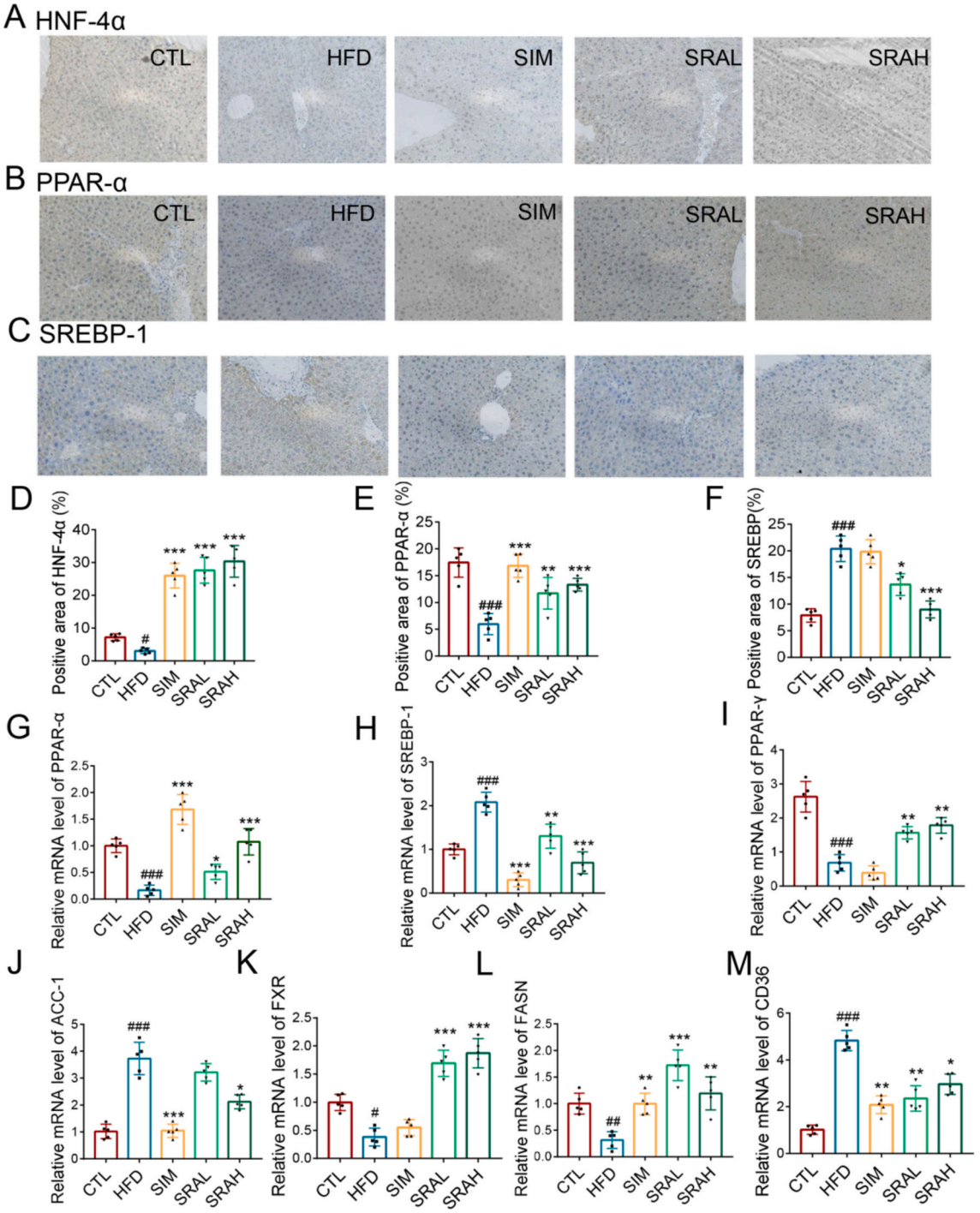

Fig. 4. SRA regulated lipid metabolism in liver cells of obese mice. Immunohistochemical analysis of HNF-4α (A), PPAR-α (B) and SREBP-1 (C) were showed (200 ×), and the positive staining areas of HNF-4α (D), PPAR-α (E) and SREBP-1 (F) was analyzed. The mRNA levels of PPAR-α (G), SREBP-1 (H), PPAR-γ (I), ACC-1 (J), FXR (K), FASN (L) and CD36 (M) were detected. All values are presented as means ± SEM ($n = 5$). Significantly different ($^{*}P < 0.05$, $^{**}P < 0.01$, $^{***}P < 0.001$) versus the HFD group. Significantly different ($\#P < 0.05$, $\#\#P < 0.01$, $\#\#\#P < 0.001$) versus the CTL group.

mechanism of SRA in regulating liver lipid metabolism, the levels of PGC-1α and the status of MAPK pathway were determined. Immunohistochemical analysis suggested that the protein level of PGC-1α was significantly lower in HFD-fed mice than in the normal diet mice, while the level of it was reversed after SRAH treatment (Fig. 5A, B), and the trend of mRNA level change in PGC-1α was consistent with it (Fig. 5C). Previous studies are consistent with the results of this study, Rius-Pérez S et al. also indicated that the PGC-1α level can lower in the obese mice liver (Rius-Perez, Torres-Cuevas, Monsalve, Miranda, & Perez, 2020). This might be caused by lack of exercise, a fat-rich diet and a polymorphism in PGC-1, which may variously combine their effects to decrease PGC-1 expression (Pessayre, 2007). Moreover, the levels of key protein in the MAPK pathway were analyzed, it was showed that the levels of phosphorylated p38, phosphorylated JNK and phosphorylated ERK-1/2 were enhanced in the liver of HFD-induced mice, suggesting that the MAPK pathway was overactivated by HFD, while it can be inhibited by SRA (Fig. 5D-G). This is consistent with existing report that obesity and saturated fatty acids decreased PGC-1 through MAPK-

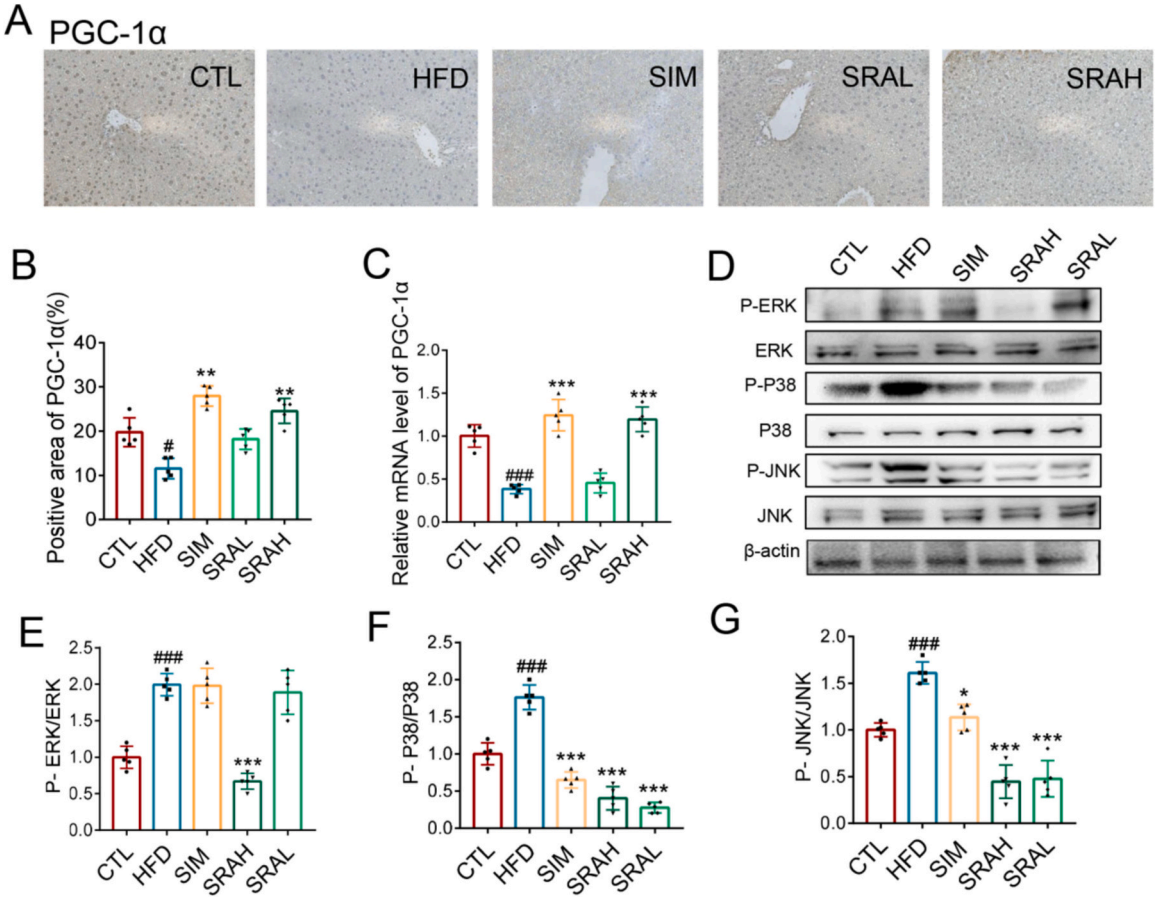

Fig. 5. SRA regulated MAPK/PGC-1α pathway in liver cells of obese mice. Immunohistochemical analysis of PGC-1α (200 ×) (A) and the positive staining area of it (B) were showed. The mRNA level of PGC-1α was detected (C). Western blotting analysis of key proteins of MAPK pathway (D). The grayscale analysis of P-ERK 1/2 (E), P—P38 (F) and P-JNK (G) were showed. All values are presented as means ± SEM ($n = 5$). Significantly different (*$P < 0.05$, **$P < 0.01$, ***$P < 0.001$) versus the HFD group. Significantly different (#$P < 0.05$, ###$P < 0.001$) versus the CTL group.

dependent transcriptional pathway (Coll et al., 2006; Crunkhorn et al., 2007). Therefore, the regulatory effect of SRA on liver lipid metabolism might be attributed to suppressing MAPK/PGC-1α pathway.

3.5. Balance of SRA on intestinal microecology

3.5.1. Improvement of intestinal microbiota homeostasis

The intestinal microbiota has been recognized as a key factor in the obesity process, and as well as an endocrine organ participated in maintaining energy homeostasis. Therefore, the effects of SRA on intestinal microbiota with HFD-treated mice were explored. Principal component analysis showed that a distinct shift of intestinal microbiota composition in mice treated with HFD, compared with mice with normal diet and SRA (Fig. 6A). At phylum level, compared with CTL group, the relative abundance of Firmicutes, Desulfobacterota and Actinobacteriota were increased, and the relative abundance of Bacteroidota and Verrucomicrobiota were decrease in the HFD group, with the intake of SRA, these abnormal changes were reversed (Fig. 6B). Further analysis revealed that 28 OTUs were screened out, their relative abundance showed significant differences in the HFD group, compared to that of the CTL group. Among them, the relative abundance of 7 OTUs were reversed by SRAL, including *Corynebacterium_stationis*, *Corynebacterium_urealyticum*, Muribaculaceae, Rikenella, *Limosilactobacillus_vaginalis*, Erysipelatoclostridiaceae and Clostridium_sensu_stricto_1 (Fig. 6C). Erysipelatoclostridiaceae was a biomarker of obesity (Hu et al., 2022), and the relative abundance of it was increased in mice with obesity, it was fortunately decreased by SRAL treatment. Previous studies have indicated that *Corynebacterium_stationis* and *Corynebacterium_urealyticum* were associated with chronic infection and liver function damage (Costales, Alsyouf, Napolitan, Wang, & Hu, 2019; Ma et al., 2021). Rikenella and Muribaculaceae were strongly associated with obesity-related parameters, for example, increase of the relative abundance of Muribaculaceae as beneficial bacteria might prevent HFD-induced metabolic disorders (Paone et al., 2022), which supports the conclusion of this study. Additionally, the intestinal microbiota participated in the integrity and function of the intestinal barrier in the homeostasis (Di Tommaso, Gasbarrini, & Ponziani, 2021). As showing in the data, the key intestinal microbiota taken part in the alleviation of HFD in mice by SRA.

3.5.2. Restoration of intestinal barrier function

Gut microbiome plays a major role in driving barrier changes. Additionally, our dietary habits influence the barrier function at different levels (Paone & Cani, 2020; Yang et al., 2022). HFD may lead to changes in the microbiota, and in the long run can further induce intestinal barrier dysfunction (Shi et al., 2020). It can also promote intestinal permeability directly or elevate barrier-disrupting cytokines indirectly (Rohr, Narasimhulu, Rudeski-Rohr, & Parthasarathy, 2020). Although the factors affecting the gut barrier have been studied for decades, the exact mechanisms are various and complementary. Herein, SRAL and SRAH treated groups showed significantly fewer damaged crypts and epithelial structures of small intestine, as well as the higher mucosal thickness and crypt depth, compared to the HFD treated group (Fig. S2A, S2C, S2D). Mice induced by HFD were companied with the decrease of the number of goblet cells and thinning of the mucous layer, which were rehabilitated after SRAL and SRAH interventions (Fig. S2B,

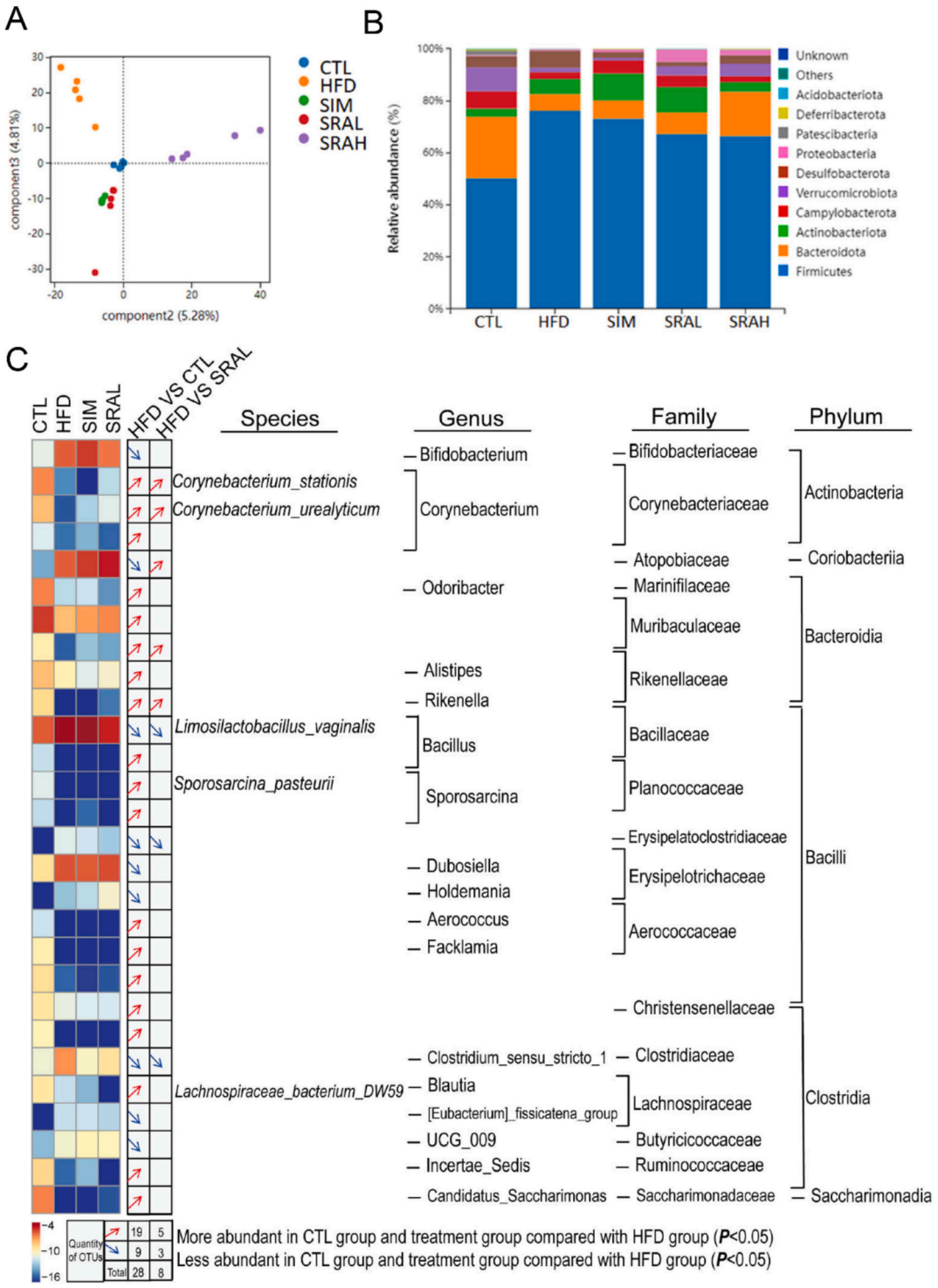

Fig. 6. SRA regulated intestinal microbiota in obese mice. PLS—DA of 16S rRNA genes (A). Composition of gut microbiota in phylum level (B). The abundance of 28 OTUs different between CTL and HFD groups was displayed by Heatmap and their detailed information (C).

S2E). To assess the protection of SRA on intestinal barrier integrity, the protein levels of tight junction genes, including zonula occludens-1 (ZO-1) and claudin-1 were analyzed. The data suggested that mice with HFD exposure possessed remarkably lower levels of ZO-1 and claudin-1 compared to mice with normal diet. SRAL and SRAH treatments exhibited an amelioration in intestinal permeability in mice with HFD, reflecting in the increased ZO-1 and claudin-1 levels (Fig. 7A-D). These data indicated that the protection of SRA on HFD induced mice involved maintenance of intestinal barriers function.

4. Conclusion

A protein rich component SRA with molecular weight mainly of 15, 40 and 50 kDa was prepared by applying wet pulverization strategy combined with temperature cycling method, which possessed the advantages of simplicity and low cost. SRA exhibited the effect on obesity control, reflecting in inhibiting lipid aggregation and steatosis in liver, and resisting proliferation of the adipocytes. The restorative mechanism of SRA might depend on regulating lipid metabolism and biosynthesis by

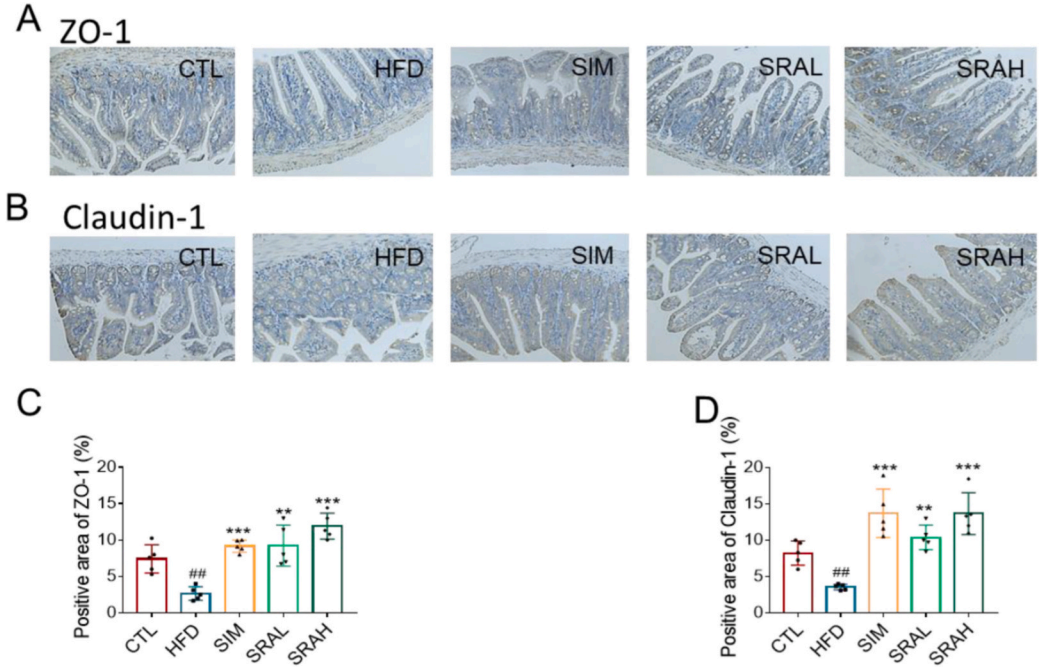

Fig. 7. SRA restored the integrity and function of the intestinal barrier in obese mice. Immunohistochemical analysis of ZO-1 (A) and Claudin-1 (B) (200 ×), and the positive staining area of them (C, D) were showed. All values are presented as means ± SEM ($n = 5$). Significantly different ($^{**}P < 0.01$, $^{***}P < 0.001$) versus the HFD group. Significantly different ($\#\#P < 0.01$) versus the CTL group.

MAPK/PGC-1α pathway. Moreover, SRA acted favorably on the intestinal barrier and relieved intestinal microbiota dysfunction in mice with HFD-induced obesity (Fig. 8). This study provides a high efficiency and low-cost method for protein extraction, and demonstrates the potential applications of *S. rugosoannulata* protein against obesity and related disorders.

CRediT authorship contribution statement

Peng Liu: Writing – original draft, Conceptualization. **Chen Gao:** Writing – original draft, Methodology. **Wen Li:** Formal analysis. **Wanchao Chen:** Methodology. **Zhong Zhang:** Data curation. **Di Wu:** Investigation. **Tingzhao Li:** Resources. **Shuai Sun:** Project administration. **Yan Yang:** Writing – review & editing, Project administration.

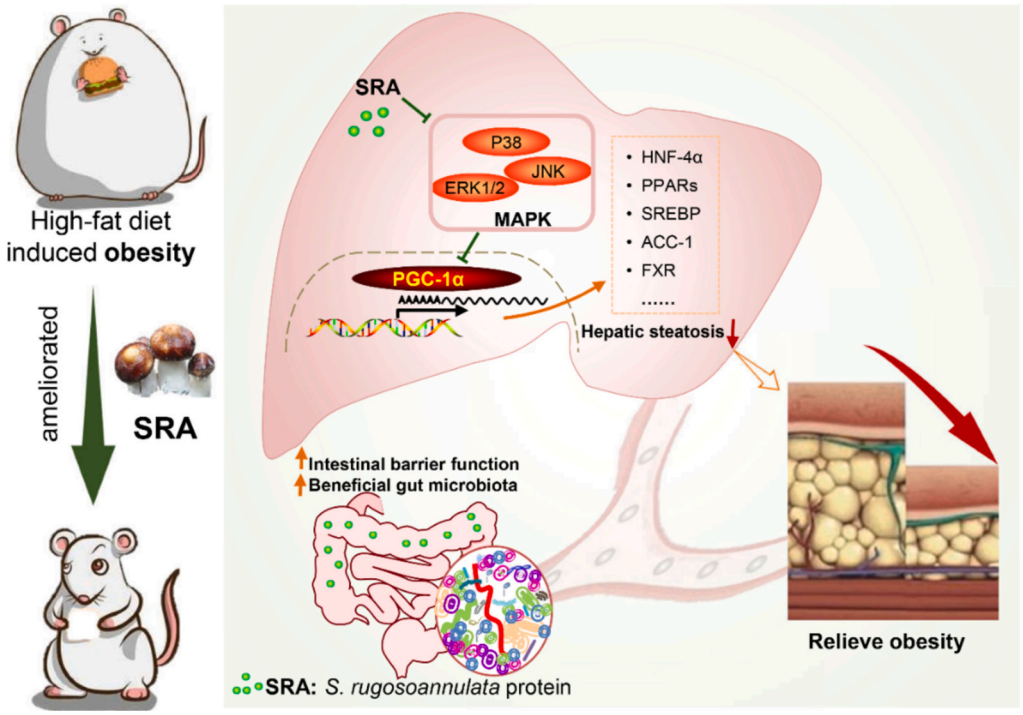

Fig. 8. The mechanism of the effect of SRA on improving obesity caused by high-fat diet.

Declaration of competing interest

The authors declare that they have no known competing financial interests or personal relationships that could have appeared to influence the work reported in this paper.

Acknowledgement

This work was supported by the National Key Research and Development Program of China (Project No 2023YFF1103401).

Appendix A. Supplementary data

Supplementary data to this article can be found online at https://doi.org/10.1016/j.fochx.2025.102170.

Data availability

data are available from the authors upon request, and the 16S rRNA data can be accessed from the Mendeley Data (https://data.mendeley.com/preview/33bfcm5d25?a=50b9a72f-8758-4ad4-a653-6b700bde33d3).

References

Ayimbila, F., & Keawsompong, S. (2023). Nutritional quality and biological application of mushroom protein as a novel protein alternative. *Current Nutrition Reports, 12*(2), 290–307. https://doi.org/10.1007/s13668-023-00468-x

Bray, G. A., Kim, K. K., Wilding, J. P. H., & World Obesity, F. (2017). Obesity: A chronic relapsing progressive disease process. A position statement of the world obesity federation. *Obesity Reviews, 18*(7), 715–723. https://doi.org/10.1111/obr.12551

Brosnan, J. T., & Brosnan, M. E. (2013). Glutamate: a truly functional amino acid. *Amino Acids, 45*(3), 413–418. https://doi.org/10.1007/s00726-012-1280-4

Cao, T. Q., An, H. X., Ma, R. J., Dai, K. Y., Ji, H. Y., Liu, A. J., & Zhou, J. P. (2023). Structural characteristics of a low molecular weight velvet antler protein and the anti-tumor activity on S180 tumor-bearing mice. *Bioorganic Chemistry, 131*, Article 106304. https://doi.org/10.1016/j.bioorg.2022.106304

Chang, C. J., Lin, C. S., Lu, C. C., Martel, J., Ko, Y. F., Ojcius, D. M., & Lai, H. C. (2015). Ganoderma lucidum reduces obesity in mice by modulating the composition of the gut microbiota. *Nature Communications, 6*, 7489. https://doi.org/10.1038/ncomms8489

Chen, Y., Nakanishi, M., Bautista, E. J., Qendro, V., Sodergren, E., Rosenberg, D. W., & Weinstock, G. M. (2020). Colon Cancer prevention with walnuts: A longitudinal study in mice from the perspective of a gut Enterotype-like cluster. *Cancer Prevention Research (Philadelphia, Pa.), 13*(1), 15–24. https://doi.org/10.1158/1940-6207.CAPR-19-0273

Cheng, C. F., Ku, H. C., & Lin, H. (2018). PGC-1alpha as a pivotal factor in lipid and metabolic regulation. *International Journal of Molecular Sciences, 19*(11). https://doi.org/10.3390/ijms19113447

Coll, T., Jove, M., Rodriguez-Calvo, R., Eyre, E., Palomer, X., Sanchez, R. M., & Vazquez-Carrera, M. (2006). Palmitate-mediated downregulation of peroxisome proliferator-activated receptor-gamma coactivator 1alpha in skeletal muscle cells involves MEK1/2 and nuclear factor-kappaB activation. *Diabetes, 55*(10), 2779–2787. https://doi.org/10.2337/db05-1494

Cong, S., Li, Z., Yu, L., Liu, Y., Hu, Y., Bi, Y., & Cheng, M. (2021). Integrative proteomic and lipidomic analysis of Kaili sour soup-mediated attenuation of high-fat diet-induced nonalcoholic fatty liver disease in a rat model. *Nutrition & Metabolism (London), 18*(1), 26. https://doi.org/10.1186/s12986-021-00553-4

Costales, J., Alsyouf, M., Napolitan, P., Wang, S., & Hu, B. (2019). Corynebacterium urealyticum: Rare urinary tract infection with serious complications. *The Canadian Journal of Urology, 26*(1), 9680–9682. https://www.ncbi.nlm.nih.gov/pubmed/30797252.

Crunkhorn, S., Dearie, F., Mantzoros, C., Gami, H., da Silva, W. S., Espinoza, D., & Patti, M. E. (2007). Peroxisome proliferator activator receptor gamma coactivator-1 expression is reduced in obesity: Potential pathogenic role of saturated fatty acids and p38 mitogen-activated protein kinase activation. *The Journal of Biological Chemistry, 282*(21), 15439–15450. https://doi.org/10.1074/jbc.M611214200

Di Ciaula, A., Baj, J., Garruti, G., Celano, G., De Angelis, M., Wang, H. H., & Portincasa, P. (2020). Liver steatosis, gut-liver Axis, microbiome and environmental factors. A never-ending bidirectional cross-talk. *Journal of Clinical Medicine, 9*(8). https://doi.org/10.3390/jcm9082648

Di Tommaso, N., Gasbarrini, A., & Ponziani, F. R. (2021). Intestinal barrier in human health and disease. *International Journal of Environmental Research and Public Health, 18*(23). https://doi.org/10.3390/ijerph182312836

Diniz, T. A., de Lima Junior, E. A., Teixeira, A. A., Biondo, L. A., da Rocha, L. A. F., Valadao, I. C., & Rosa Neto, J. C. (2021). Aerobic training improves NAFLD markers and insulin resistance through AMPK-PPAR-alpha signaling in obese mice. *Life Sciences, 266*, Article 118868. https://doi.org/10.1016/j.lfs.2020.118868

Gao, Y., Abuduaini, G., Yang, C., Zhang, S., Zhang, Y., Fan, H., & Liu, T. (2022). Isolation, purification, and structural elucidation of Stropharia rugosoannulata polysaccharides with hypolipidemic effect. *Frontiers in Nutrition, 9*, 1092582. https://doi.org/10.3389/fnut.2022.1092582

Gonzalez, A., Cruz, M., Losoya, C., Nobre, C., Loredo, A., Rodriguez, R., & Belmares, R. (2020). Edible mushrooms as a novel protein source for functional foods. *Food & Function, 11*(9), 7400–7414. https://doi.org/10.1039/d0fo01746a

Gu, H., An, H. J., Gwon, M. G., Bae, S., Zouboulis, C. C., & Park, K. K. (2022). *The effects of synthetic SREBP-1 and PPAR-gamma decoy Oligodeoxynucleotide on acne-like disease in vivo and in vitro via Lipogenic regulation. Biomolecules, Vol. 12(12)*. https://doi.org/10.3390/biom12121858

Haemmerle, G., Moustafa, T., Woelkart, G., Buttner, S., Schmidt, A., van de Weijer, T., & Zechner, R. (2011). ATGL-mediated fat catabolism regulates cardiac mitochondrial function via PPAR-alpha and PGC-1. *Nature Medicine, 17*(9), 1076–1085. https://doi.org/10.1038/nm.2439

Hu, J., Guo, P., Mao, R., Ren, Z., Wen, J., Yang, Q., & Liu, Y. (2022). Gut microbiota signature of obese adults across different classifications. *Diabetes Metab Syndr Obes, 15*, 3933–3947. https://doi.org/10.2147/DMSO.S387523

Jin, M., Shen, Y., Pan, T., Zhu, T., Li, X., Xu, F., & Zhou, Q. (2021). Dietary betaine mitigates hepatic steatosis and inflammation induced by a high-fat-diet by modulating the Sirt1/Srebp-1/Ppara pathway in juvenile black seabream (Acanthopagrus schlegelii). *Frontiers in Immunology, 12*, Article 694720. https://doi.org/10.3389/fimmu.2021.694720

Kolhe, P., Amend, E., & Singh, S. K. (2010). Impact of freezing on pH of buffered solutions and consequences for monoclonal antibody aggregation. *Biotechnology Progress, 26*(3), 727–733. https://doi.org/10.1002/btpr.377

Li, J., Wu, H., Liu, Y., & Yang, L. (2020). High fat diet induced obesity model using four strainsof mice: Kunming, C57BL/6. *BALB/c and ICR. Exp Anim, 69*(3), 326–335. https://doi.org/10.1538/expanim.19-0148

Li, W., Chen, W., Ma, H., Wu, D., Zhang, Z., & Yang, Y. (2022). Structural characterization and angiotensin-converting enzyme (ACE) inhibitory mechanism of Stropharia rugosoannulata mushroom peptides prepared by ultrasound. *Ultrasonics Sonochemistry, 88*, Article 106074. https://doi.org/10.1016/j.ultsonch.2022.106074

Li, Y., Zalzala, M., Jadhav, K., Xu, Y., Kasumov, T., Yin, L., & Zhang, Y. (2016). Carboxylesterase 2 prevents liver steatosis by modulating lipolysis, endoplasmic reticulum stress, and lipogenesis and is regulated by hepatocyte nuclear factor 4 alpha in mice. *Hepatology, 63*(6), 1860–1874. https://doi.org/10.1002/hep.28472

Liang, H., & Ward, W. F. (2006). PGC-1alpha: A key regulator of energy metabolism. *Advances in Physiology Education, 30*(4), 145–151. https://doi.org/10.1152/advan.00052.2006

Liu, F., Chen, S., Li, X., Li, S., Xiao, Y., Han, J., & Yu, H. (2023). Obesity-induced hepatic steatosis is partly mediated by visceral fat accumulation in subjects with overweight/obesity: A cross-sectional study. *Obesity Facts, 16*(2), 164–172. https://doi.org/10.1159/000527595

Liu, P., Li, H., Xu, H., Gong, J., Jiang, M., Xu, Z., & Shi, J. (2023). Aggravated hepatic fibrosis induced by phenylalanine and tyrosine was ameliorated by chitooligosaccharides supplementation. *iScience, 26*(10), Article 107754. https://doi.org/10.1016/j.isci.2023.107754

Luo, S. Y., Huang, Z., Chen, X., Zong, M. H., & Lou, W. Y. (2023). Extraction and characterization of a functional protein from Millettia speciosa champ. Leaf. *Natural Product Research, 37*(1), 31–38. https://doi.org/10.1080/14786419.2021.1947271

Ma, J., Gong, S., He, Y., Gao, W., Hao, W., & Lan, X. (2021). Effects of oral sialic acid on gut development, liver function and gut microbiota in mice. *Letters in Applied Microbiology, 73*(1), 20–25. https://doi.org/10.1111/lam.13447

Marco, A., Rubio, R., Compano, R., & Casals, I. (2002). Comparison of the Kjeldahl method and a combustion method for total nitrogen determination in animal feed. *Talanta, 57*(5), 1019–1026. https://doi.org/10.1016/s0039-9140(02)00136-4

Oropeza, D., Jouvet, N., Bouyakdan, K., Perron, G., Ringuette, L. J., Philipson, L. H., & Estall, J. L. (2015). PGC-1 coactivators in beta-cells regulate lipid metabolism and are essential for insulin secretion coupled to fatty acids. *Molecular Metabolism, 4*(11), 811–822. https://doi.org/10.1016/j.molmet.2015.08.001

Paone, P., & Cani, P. D. (2020). Mucus barrier, mucins and gut microbiota: The expected slimy partners? *Gut, 69*(12), 2232–2243. https://doi.org/10.1136/gutjnl-2020-322260

Paone, P., Suriano, F., Jian, C., Korpela, K., Delzenne, N. M., Van Hul, M., & Cani, P. D. (2022). Prebiotic oligofructose protects against high-fat diet-induced obesity by changing the gut microbiota, intestinal mucus production, glycosylation and secretion. *Gut Microbes, 14*(1), 2152307. https://doi.org/10.1080/19490976.2022.2152307

Pessayre, D. (2007). Role of mitochondria in non-alcoholic fatty liver disease. *Journal of Gastroenterology and Hepatology, 22*(Suppl. 1), S20–S27. https://doi.org/10.1111/j.1440-1746.2006.04640.x

Rius-Perez, S., Torres-Cuevas, I., Monsalve, M., Miranda, F. J., & Perez, S. (2020). Impairment of PGC-1 alpha up-regulation enhances Nitrosative stress in the liver during acute pancreatitis in obese mice. *Antioxidants (Basel), 9*(9). https://doi.org/10.3390/antiox9090887

Rohr, M. W., Narasimhulu, C. A., Rudeski-Rohr, T. A., & Parthasarathy, S. (2020). Negative effects of a high-fat diet on intestinal permeability: A review. *Advances in Nutrition, 11*(1), 77–91. https://doi.org/10.1093/advances/nmz061

S, K., & J, B. (1978). Vibrational spectroscopy and conformation of peptides, polypeptides, and proteins. *L'Unión Médicale du Canada, 107*(8), 767. https://www.ncbi.nlm.nih.gov/pubmed/354153.

Shi, H., Yu, Y., Lin, D., Zheng, P., Zhang, P., Hu, M., & Huang, X. F. (2020). beta-glucan attenuates cognitive impairment via the gut-brain axis in diet-induced obese mice. *Microbiome, 8*(1), 143. https://doi.org/10.1186/s40168-020-00920-y

Spagnuolo, R., Montalcini, T., De Bonis, D., Ferro, Y., Cosco, C., Mazza, E., & Pujia, A. (2019). Weight gain and liver steatosis in patients with inflammatory bowel diseases. *Nutrients, 11*(2). https://doi.org/10.3390/nu11020303

Sun, Q., Ma, J., Campos, H., Hankinson, S. E., Manson, J. E., Stampfer, M. J., & Hu, F. B. (2007). A prospective study of trans fatty acids in erythrocytes and risk of coronary heart disease. *Circulation, 115*(14), 1858–1865. https://doi.org/10.1161/CIRCULATIONAHA.106.679985

Tatulian, S. A. (2019). FTIR analysis of proteins and protein-membrane interactions. *Methods in Molecular Biology, 2003*, 281–325. https://doi.org/10.1007/978-1-4939-9512-7_13

Tiwari, S. C., & Suprenant, K. A. (1993). A pH- and temperature-dependent cycling method that doubles the yield of microtubule protein. *Analytical Biochemistry, 215*(1), 96–103. https://doi.org/10.1006/abio.1993.1560

Xie, Y., Zhang, H., Liu, H., Xiong, L., Gao, X., Jia, H., & Han, T. (2015). Hypocholesterolemic effects of Kluyveromyces marxianus M3 isolated from Tibetan mushrooms on diet-induced hypercholesterolemia in rat. *Brazilian Journal of Microbiology, 46*(2), 389–395. https://doi.org/10.1590/S1517-838246220131278

Xu, L., Wang, X., Xu, Y., Meng, J., Feng, C., Geng, X., & Chang, M. (2023). Effects of freeze-thaw cycles on the structures and functional properties of Clitocybe squamulosa protein isolates. *Foods, 12*(15). https://doi.org/10.3390/foods12152948

Yan, L., Sundaram, S., Rust, B. M., Palmer, D. G., Johnson, L. K., & Zeng, H. (2022). Consumption of a high-fat diet alters transcriptional rhythmicity in liver from pubertal mice. *Frontiers in Nutrition, 9*, 1068350. https://doi.org/10.3389/fnut.2022.1068350

Yang, J., Wei, H., Zhou, Y., Szeto, C. H., Li, C., Lin, Y., & Yu, J. (2022). High-fat diet promotes colorectal tumorigenesis through modulating gut microbiota and metabolites. *Gastroenterology, 162*(1), 135–149 e132. https://doi.org/10.1053/j.gastro.2021.08.041

Zhang, J., Liu, M., Deng, H., Zhao, Y., Zhu, Y., Bai, J., & Xiao, X. (2022). Purification and identification of lipid-lowering protein from barley extract after Lactiplantibacillus plantarum dy-1 fermentation. *Journal of Agricultural and Food Chemistry, 70*(45), 14488–14498. https://doi.org/10.1021/acs.jafc.2c05211

Zhang, M., Bai, X., Du, Q., Xu, J., Wang, D., Chen, L., & Yang, J. (2023). The different mechanisms of lipid accumulation in hepatocytes induced by oleic acid/palmitic acid and high-fat diet. *Molecules, 28*(18). https://doi.org/10.3390/molecules28186714

Zhang, Y., Castellani, L. W., Sinal, C. J., Gonzalez, F. J., & Edwards, P. A. (2004). Peroxisome proliferator-activated receptor-gamma coactivator 1alpha (PGC-1alpha) regulates triglyceride metabolism by activation of the nuclear receptor FXR. *Genes & Development, 18*(2), 157–169. https://doi.org/10.1101/gad.1138104

Zhao, S., Rong, C., Liu, Y., Xu, F., Wang, S., Duan, C., & Wu, X. (2015). Extraction of a soluble polysaccharide from Auricularia polytricha and evaluation of its anti-hypercholesterolemic effect in rats. *Carbohydrate Polymers, 122*, 39–45. https://doi.org/10.1016/j.carbpol.2014.12.041